

What are we learning from simulating wall turbulence?

BY JAVIER JIMÉNEZ^{1,2,*} AND ROBERT D. MOSER³

¹*School of Aeronautics, Universidad Politécnica de Madrid,
28040 Madrid, Spain*

²*Centre for Turbulence Research, Stanford University,
Building 500, Stanford, CA 94305-3035, USA*

³*Department of Mechanical Engineering and Institute for Computational
Engineering and Sciences, University of Texas at Austin,
Austin, TX 78735, USA*

The study of turbulence near walls has experienced a renaissance in the last decade, largely owing to the availability of high-quality numerical simulations. The viscous and buffer layers over smooth walls are essentially independent of the outer flow, and there is a family of numerically exact nonlinear structures that account for about half of the energy production and dissipation. The rest can be modelled by their unsteady bursting. Many characteristics of the wall layer, such as the dimensions of the dominant structures, are well predicted by those models, which were essentially completed in the 1990s after the increase in computer power made the kinematic simulations of the late 1980s cheap enough to undertake dynamic experiments.

Today, we are at the early stages of simulating the logarithmic (or overlap) layer, and a number of details regarding its global properties are becoming clear. For instance, a finite Reynolds number correction to the logarithmic law has been validated in turbulent channels. This has allowed upper and lower limits of the overlap region to be clarified, with both upper and lower bounds occurring at much larger distances from the wall than commonly assumed. A kinematic picture of the various cascades present in this part of the flow is also beginning to emerge. Dynamical understanding can be expected in the next decade.

Keywords: wall turbulence; numerical simulations; logarithmic layer; permanent waves

1. Introduction

Some of the first systems in which turbulence was identified were wall-bounded flows (Hagen 1839; Darcy 1854), but to date they remain poorly understood compared with homogeneous or free-shear turbulence. Part of the reason is that we are interested in different things in each case. While the emphasis away from walls is

* Author for correspondence (jimenez@torroja.dmt.upm.es).

One contribution of 14 to a Theme Issue ‘Scaling and structure in high Reynolds number wall-bounded flows’.

on the self-similar energy cascade (Kolmogorov 1941) or in the energy-containing structures controlled by large-scale instabilities (Brown & Roshko 1974), wall-bounded turbulence is essentially inhomogeneous and anisotropic. The eddies containing most of the energy at one wall distance are in the midst of the inertial cascade when they are observed farther away from the wall. The local Reynolds number, defined as the scale disparity between energy and dissipation, also changes with the wall distance. The main emphasis in wall turbulence is not so much on the energy cascade between eddies at the same geometric location, which is probably similar to that in other turbulent flows, but on the interplay between different scales at different distances from the wall.

A particularly simple part of wall-bounded turbulent flows is the thin near-wall region formed by the viscous and the buffer layers in the immediate vicinity of smooth walls, where viscosity is important and the energetic and dissipative scales overlap. This layer, although geometrically negligible when compared with the bulk of the flow, is both technologically and scientifically important, because a relatively large fraction of the velocity difference across boundary layers resides in it. Its modern study began experimentally by Kim *et al.* (1971) and Morrison *et al.* (1971) in the 1970s, and got a strong impulse with the advent of the first high-quality direct numerical simulations by Kim *et al.* (1987) in the late 1980s and 1990s.

The logarithmic layer is located just above that region, and it is also unique to wall turbulence. It has been studied experimentally for a long time, but its numerical simulation is only now beginning to be possible. It is still poorly understood compared with the viscous layers.

The numerical emphasis of the present review is partly a personal bias of the authors, but it is not altogether arbitrary. When direct numerical simulations are possible, they allow much more general ‘instrumentation’, but more importantly they allow non-physical numerical ‘experiments’ to probe turbulence dynamics in a way not possible in the laboratory. However, the simulations are limited in Reynolds number, and for this reason, the near-wall region is well suited to numerical investigation. It has also been difficult to explore experimentally, so much of the available information is numerical. We explore here what can be learned from this rich source of information. There is also a large, valuable and complementary experimental literature on wall-bounded turbulence, which covers a larger range of Reynolds numbers and uses continuously improving instrumentation; see the papers in this special issue for reviews.

This paper is organized as follows. In §2, we define the near-wall layer and outline the classical models for it. In §3, we review the recent work on equilibrium solutions for wall-bounded shear flows and how they are related to turbulence, and in §4, we discuss briefly the present status of our understanding of the logarithmic layer. Finally some conclusions are offered.

2. The structure of near-wall turbulence

Wall-bounded turbulence over smooth walls can be described to a good approximation in terms of two sets of scaling parameters (Tennekes & Lumley 1972). Viscosity is important near the wall, and the units for length and velocity are constructed with the kinematic viscosity ν and the friction velocity

$u_\tau = (\tau_w/\rho)^{1/2}$, which is based on the shear wall stress τ_w and the fluid density ρ . Magnitudes expressed in these ‘wall units’ are denoted by ⁺ superscripts. The wall distance y^+ can, for example, be interpreted as a Reynolds number for wall-attached eddies. Viscosity remains relevant up to $y^+ \approx 150$ (Österlund *et al.* 2000), and it is owing to those relatively low values that this region is a good candidate for simple modelling.

Farther from the wall, the velocity also scales approximately with u_τ but the length-scale is the flow thickness h . Between the inner and the outer regions, there is an intermediate layer where the only length-scale is the wall distance y . The mean velocity in that ‘logarithmic’ layer is given approximately by

$$U^+ = \kappa^{-1} \log y^+ + B. \quad (2.1)$$

The Kármán constant $\kappa \approx 0.4$ is approximately universal. The intercept constant is $B \approx 5$ for smooth walls, but depends on the details of the near-wall region.

The two viscous inner layers are extremely important for the flow as a whole. If h is the half-height in channels, the boundary layer thickness, or the pipe radius, the ratio between the inner and the outer length-scales is the friction Reynolds number, h^+ , which ranges from 200 for barely turbulent flows to $h^+ = 5 \times 10^5$ for large water pipes. In the latter, the near-wall layer is only approximately 3×10^{-4} times the pipe radius, but it follows from (2.1) that 40% of the velocity drop takes place below $y^+ = 50$. Turbulence is characterized by the expulsion towards the small scales of the energy dissipation, away from the energy-containing eddies. In wall-bounded flows, this separation occurs not only in the scales of the velocity fluctuations, but also in the mean velocity profile from the centre of the flow towards the walls.

Owing to this ‘singular’ nature, the near-wall layer is not only important for the rest of the flow, but it is also essentially independent from it. This was shown by numerical experiments with ‘autonomous’ simulations by Jiménez & Pinelli (1999), where the outer flow was artificially removed above a certain wall distance δ . The near-wall dynamics was unaffected as long as $\delta^+ \geq 60$, at least when compared with low-Reynolds number flows. We will see below that there is some influence of the outer flow even in the viscous sublayer, but it happens at scales which are different from those of the typical inner layer dynamics.

Most of the velocity difference that does not reside in the near-wall region is concentrated in the logarithmic layer, which extends experimentally up to $y = 0.2h$ (figure 1). It follows from (2.1) that the velocity difference above this limit is only 20% of the total when $h^+ \approx 200$, and decreases logarithmically for higher Reynolds numbers. In the limit of infinite Reynolds number, all the velocity drop is in the logarithmic layer.

The buffer, viscous and logarithmic layers are the most characteristic features of wall-bounded flows, and they constitute the main difference between them and other types of turbulence. The first two layers are today relatively easy to compute, because the local Reynolds numbers are low, and we will see below that they can be described in terms of relatively simple eddies. Owing to the velocity estimates in the previous paragraphs, understanding those layers has practical implications. They are, for example, responsible for most of the friction drag at moderate Reynolds numbers, and any attempt to control wall friction has to centre on them.

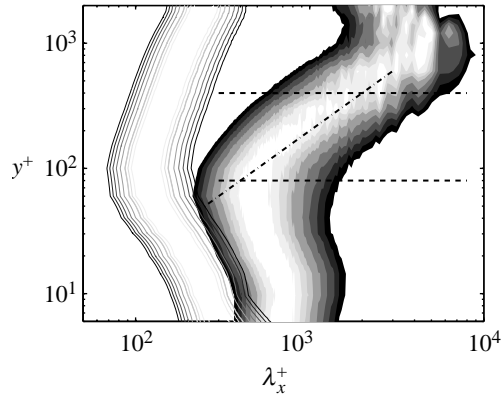


Figure 1. Pre-multiplied spectra, $kE(k)$, of the kinetic energy, $|u'|^2$ (shaded), and of the entropy, $|\omega'|^2$ (lines), as functions of the streamwise wavelength $\lambda_x = 2\pi/k_x$, and of the wall distance, y . At each y , the lowest contour is 0.86 times the local maximum. The two horizontal lines are the $y^+ = 80$ and $y/h = 0.2$, and represent the limits of the logarithmic layer. The diagonal line is $\lambda_x = 2y$. Channel by Hoyas & Jiménez (2006). $h^+ = 2000$.

The logarithmic layer, on the other hand, is an intrinsically high-Reynolds number region. Its existence requires at least that its upper limit should be above the lower one, so that $0.2h^+ \geq 100$ and $h^+ \geq 500$. Owing to this, numerical simulations with an appreciable logarithmic region have only recently become available (del Álamo *et al.* 2004; Hoyas & Jiménez 2006).

(a) *The classical model*

The region below $y^+ \approx 100$ has been intensively studied. It is dominated by coherent streaks of the streamwise velocity and by quasi-streamwise vortices. The former are an irregular array of long ($x^+ \approx 10^3 - 10^4$) sinuous alternating streamwise jets superimposed on the mean shear, with an average spanwise separation of the order of $z^+ \approx 100$ (Smith & Metzler 1983). The vortices are slightly tilted away from the wall (Jeong *et al.* 1997) and stay in the near-wall region only for $x^+ \approx 200$. Several vortices are associated with each streak (Jiménez & Moin 1991), with a longitudinal spacing of the order of $x^+ \approx 400$. Most of them merge into disorganized vorticity outside the immediate neighbourhood of the wall (Robinson 1991).

It was proposed very early that streaks and vortices were involved in a mutual regeneration cycle in which the vortices were the results of instability of the streaks (Swearingen & Blackwelder 1987), while the streaks were caused by the advection of the mean velocity gradient by the vortices (Bakewell & Lumley 1967; Kim *et al.* 1971). There is still some discussion on how the vortices are generated, but it is known that they derive from the streaks, because disturbing the latter inhibits their formation (Jiménez & Pinelli 1999). This manipulation is only effective between $y^+ \approx 60$ and 10, suggesting that the streaks are involved in the vortex-generation process mostly within that region. Numerical (Hamilton *et al.* 1995; Waleffe 1997; Schoppa & Hussain 2002) and analytical (Reddy *et al.* 1998; Kawahara *et al.* 2003) work on model streaks shows that they are linearly unstable to a variety of sinuous perturbations, associated with inflection points of

the perturbed velocity profile, whose eigenfunctions correspond well with the shape and the location of the observed vortices. The model implied by these instabilities is a time-dependent cycle in which streaks and vortices grow, generate each other and eventually decay. Jiménez & Pinelli (1999) discuss other unsteady models of this type and give additional references.

3. Exact solutions for the sublayer

A slightly different point of view is that the regeneration cycle is organized around a nonlinear travelling wave, a fixed point in some phase space, representing a non-uniform streak. This is actually not too different from the previous model, which essentially assumes that the undisturbed streak is a fixed point in phase space, and that the cycle is an approximation to an orbit along its unstable manifold. The new model, however, considers fixed points which are non-trivially perturbed streaks and separates the dynamics of turbulence from that of transition.

The organization of the buffer layer does not require the chaos observed in fully turbulent flows. Simulations in which the flow is substituted by an ordered array of identical structures reproduce the correct statistics (Jiménez & Moin 1991). In a further simplification, which occurred at roughly the same time as the previous one, nonlinear equilibrium solutions of the three-dimensional Navier–Stokes equations were obtained numerically by Nagata (1990), with characteristics which suggested that they could be useful in describing the near-wall region. Other such solutions were later found for plane Couette flow (Waleffe 2003), plane Poiseuille flow (Toh & Itano 2001; Waleffe 2001, 2003), and for an autonomous wall flow (Jiménez & Simens 2001). All of them look qualitatively similar (Waleffe 1998; Kawahara *et al.* 2003), and contain a wavy low-velocity streak flanked by a pair of staggered quasi-streamwise vortices of alternating signs, closely resembling the spatially coherent objects deduced from the near-wall region of true turbulence. An example is shown in figure 2. Their mean and fluctuation intensity profiles are reminiscent of experimental values (Jiménez & Simens 2001; Waleffe 2003), as shown in figure 3*a*, and the range of spanwise wavelengths in which they exist is in the neighbourhood of the observed spacing of the streaks in the sublayer (Jiménez *et al.* 2005).

In those cases in which the stability of the equilibrium solutions has been investigated, they have been found to be unstable saddles in phase space at the Reynolds numbers at which turbulence is observed. They are not therefore expected to exist as such in real turbulence, but any turbulent flow could spend a substantial fraction of its lifetime in their neighbourhood. Exact limit cycles and heteroclinic orbits based on these fixed points have been found numerically (Kawahara & Kida 2001; Toh & Itano 2003), and several reduced dynamical models of the near-wall region have been formulated in terms of low-dimensional projections of such solutions (Aubry *et al.* 1988; Sirovich & Zhou 1994; Waleffe 1997). Such unsteadiness is an important part of wall turbulence. Jiménez *et al.* (2005) showed that a well-defined bursting cycle can be identified both in simplified solutions and in fully turbulent flows, and that the unsteadiness accounts for roughly 50% of the production and dissipation of turbulent energy in the buffer region.

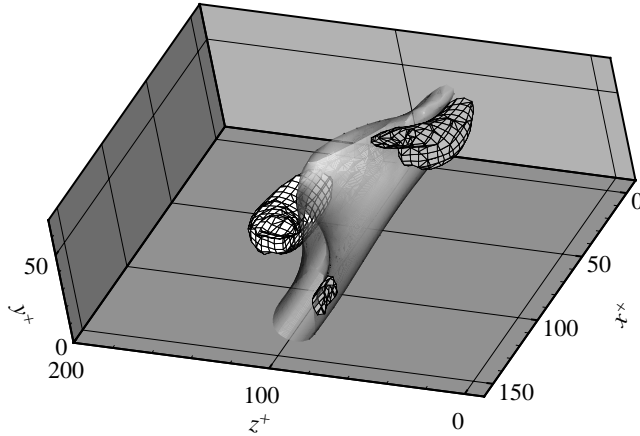


Figure 2. Exact permanent-wave solution for the Navier–Stokes equations in an ‘autonomous’ domain below $\delta^+ = 40$. The flow is from top-right to bottom-left. The central object is an isosurface of the streamwise perturbation velocity, $\bar{u}^+ = -3.5$, and defines the streak. It is flanked by two staggered streamwise vortices of opposite signs, $\omega_x^+ = \pm 0.18$, whose effect is to create an upwash that maintains the streak (Jiménez & Simens 2001).

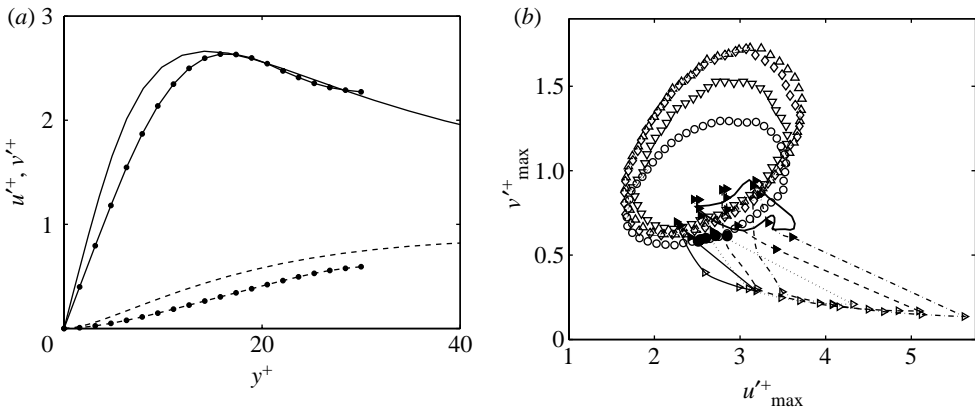


Figure 3. (a) Profiles of the root-mean-square velocity fluctuations in a channel (Kim *et al.* 1987) with $h^+ = 180$ (without symbols), and in the permanent-wave solution in figure 2 (symbols). Straight line represents streamwise velocity; dashed line represents wall-normal velocity. (b) Comparison of the maxima of the u' and v' profiles of some exact solutions with near-wall turbulence, taken over boxes of size $x^+ \times z^+ \times y^+ = 380 \times 110 \times 50$. Line of triangles represent Couette flow, at different Reynolds numbers (Jiménez *et al.* 2005). Solid symbols are ‘upper branch’ solutions, and open ones are ‘lower branch’. Filled circles represent autonomous permanent waves (Jiménez & Simens 2001). The solid loop is a limit cycle in plane Couette flow (Kawahara & Kida 2001). Other symbols are 90% probability isocontours from large numerical channels (del Álamo & Jiménez 2003; del Álamo *et al.* 2004): upward open triangle, $h^+ = 1880$; open rhombus, 950; downward open triangle, 550; open circle, 180.

Another question is whether all the exact solutions that have been published for wall-bounded flows are related to each other and to near-wall turbulence. This is addressed in figure 3*b*, taken from Jiménez *et al.* (2005). The earliest and best-understood non-trivial steady solutions of a wall-bounded Navier–Stokes

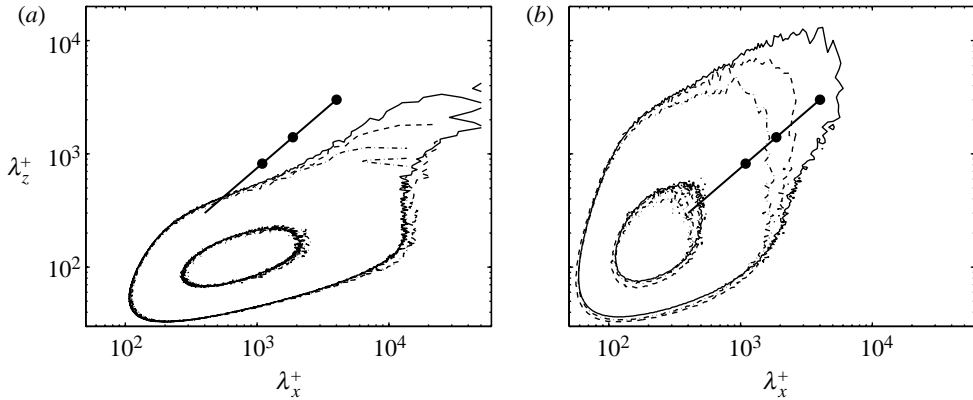


Figure 4. Spectral energy density, $k_x k_z E(k_x, k_z)$, in the near-wall region ($y^+ = 15$) of (a) streamwise velocity and (b) pressure, in terms of the streamwise and spanwise wavelengths. Numerical channels (del Álamo & Jiménez 2003; del Álamo *et al.* 2004; Hoyas & Jiménez 2006). Dash-dotted line, $h^+ = 547$; dashed line, 934; straight line, 2003. Spectra are normalized in wall units, and the contours are 0.125 and 0.625 times the maximum of the spectrum for the highest Reynolds number. The straight line is $\lambda_z = 0.75\lambda_x$, and the heavy dots are $\lambda_z = 1.5h$ for the three cases.

shear flow are those by Nagata (1990) for plane Couette flow. They can be classified into ‘upper’ and ‘lower’ branches in terms of their mean wall shear, and Jiménez *et al.* (2005) showed that this classification can be extended to most of the other known wall-bounded steady solutions. Both branches have very different characteristics. The ‘upper’ solutions have relatively weak sinuous streaks flanked by strong vortices. They consequently have relatively weak root-mean-square streamwise-velocity fluctuations u' , and strong wall-normal ones v' , at least when compared with those in the lower branch. The solution in figure 2 belongs to the upper branch, and we already saw in figure 3a that its r.m.s. velocity fluctuations profiles agree well with those of a full channel. ‘Lower’ solutions have stronger and essentially straight streaks and much weaker vortices.

The relative strength of both the types of fluctuations for a particular solution can be characterized by the maximum values of its u' and v' profiles, both of which are usually attained within the near-wall layer. Those two numbers can then be used to compare different solutions among themselves, and with fully turbulent flows. This is done in figure 3b, which compares single points from individual equilibrium solutions, with probability density functions of the statistics taken over sub-boxes of similar size in fully turbulent large-box simulations.

The results of the figure suggest that only the ‘upper-branch’ exact solutions are representative of real turbulence, at least at the scales corresponding to a single streak and to a single vortex pair. They also show that the correspondence is reasonably good for the weaker turbulent fluctuations. As mentioned above, stronger fluctuations correspond to unsteady bursting.

(a) The failure of wall scaling

Note that the probability densities in figure 3b depend on the Reynolds number, but they saturate beyond approximately $h^+ = 1000$. The same is not true for the velocity fluctuation profiles compiled over full flows, instead of

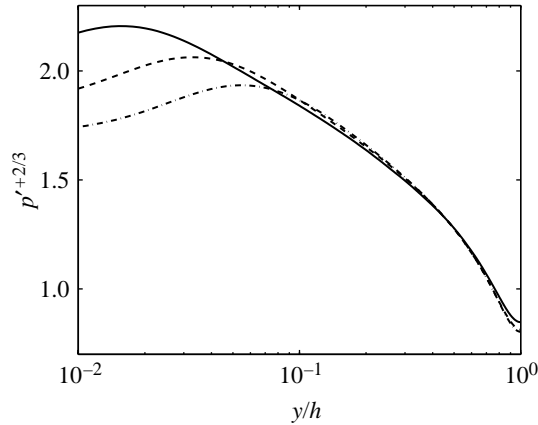


Figure 5. Intensity of the fluctuations of static pressure for the numerical channels in figure 4. Lines as in that figure.

over small sub-boxes, which keep increasing as the Reynolds number grows (DeGraaf & Eaton 2000). That effect is due to large outer flow velocity fluctuations reaching the wall (del Álamo & Jiménez 2003; Jiménez *et al.* 2004), and is unrelated to the structures considered in §3.

This is shown in figure 4a, which contains two-dimensional pre-multiplied energy spectra of the streamwise velocity, displayed as functions of the streamwise and the spanwise wavelengths. The three spectra correspond to large numerical channels at different Reynolds numbers. The lower left corner contains the streamwise velocity streaks discussed above, which are very approximately universal and local to the near-wall layer. They have widths of the order of $z^+ = 100$, and total lengths $x^+ \approx 10^4$, independent of the Reynolds number. The spectra differ from each other almost exclusively in the long and wide structures represented in the upper right corner of the spectrum, whose sizes are of the order of $\lambda_x \times \lambda_z = 10h \times h$ (del Álamo & Jiménez 2003; Jiménez *et al.* 2004; Hoyas & Jiménez 2006). Those structures extend into the logarithmic layer, scale in outer units, and correspond approximately to the ‘attached eddies’ proposed by Townsend (1976). Since they are too large to be contained within the averaging boxes used in §3, they do not influence the statistics in figure 3b.

The most obvious interaction between the inner and outer layers is through the pressure, which is a global quantity that has long been suspected of not scaling in wall units (Townsend 1976, p. 168). It was also soon realized that a failure of the pressure scaling should translate into a similar failure in the velocities, since the pressure fluctuations would drive wall-parallel ‘inactive’ motions (Bradshaw 1967).

The pressure spectra for three Reynolds numbers are displayed in figure 4b. They can be integrated to obtain the intensity of the pressure fluctuations, which turns out to depend on $\log(y/h)$, because only eddies whose sizes are between y and h contribute to the pressure at a given point. The logarithm comes about because the pressure satisfies a Poisson equation whose right-hand side is a combination of squares of the velocity gradients (Bradshaw & Koh 1981), which

behave like u_τ/y in the overlap layer. Their integration results in

$$p'^2(y) \sim u_\tau^4 \log^3\left(\frac{y}{h}\right). \quad (3.1)$$

This behaviour is confirmed by figure 5. The maximum fluctuation is at the top of the viscous layer, where p'^2 is proportional to $\log^3(h^+)$. This agrees qualitatively with a recent survey of pressure fluctuations at the wall by Hu *et al.* (2006), who found that p'^2_w scales linearly with $\log(h^+)$. The difference in the exponents of the logarithm is not significant, because the range of experimental Reynolds numbers is not enough to distinguish among exponents of $O(1)$. In fact, even if Hu *et al.* (2006) propose a linear law in their text, their graphic compilation suggests a quadratic one. A similar scaling ambiguity was found for the velocity fluctuations by del Álamo *et al.* (2004).

It follows from (2.1) that $U_\infty^+ \sim \log(h^+)$ and logarithmic scalings are sometimes interpreted as ‘mixed’ scalings with some power of U_∞ . From the argument above, we believe that the logarithm is the correct quantity. Rough walls, where the additive constant of (2.1) can be much smaller than the smooth ones, can distinguish between the two interpretations. Flores & Jiménez (2006) collected data for the velocity fluctuations over both the types of walls, and found that the logarithm is in that case a much better scale than U_∞^+ .

In this view, the scaling failure for some quantities near the wall is due to the divergence at the wall of the Poisson integral for the pressure, which would be logarithmically singular at infinite Reynolds number. The better-known scaling failure of U_∞^+ is due to a similar divergence of the integral of the mean velocity gradient.

4. The logarithmic layer

We noted in §1 that the logarithmic layer is expensive to compute. The first simulations with an appreciable logarithmic range have only appeared in the last few years, and even in them the extent of the log layer is limited. Further, there has been recent controversy regarding the limits of the logarithmic law, the constants and even the functional form of the mean velocity profile. There is thus some uncertainty regarding conditions under which a log layer is expected, and its properties. This issue is addressed here by exploring finite Reynolds number effects in the log layer.

(a) *The mean velocity in the logarithmic layer*

The logarithmic velocity profile first deduced by Millikan (1938) was later reinterpreted as arising from a high Reynolds number asymptotic analysis (Yajnik 1970; Mellor 1972; Phillips 1987). In essence, the logarithmic law is the matching condition in a multi-scale asymptotic analysis, in which the small inner scale is the wall unit (ν/u_τ), and the large outer scale is (in the channel) the channel half-width h . As the leading term in an asymptotic approximation, it is strictly valid only in the limit of infinite Reynolds number. However, since all experiments and computations are at finite Reynolds number, it is of great practical importance to determine how this asymptotic limit is approached with increasing Reynolds number, so that the finite Reynolds number of available observations can be accounted for. To this end, Afzal & Yajnik (1973) and

Afzal (1976) extended the asymptotic analysis for channels and pipes to include the lowest order finite Reynolds number effects in the overlap region, and Phillips (1987) pursued a somewhat different asymptotic approach in boundary layers with the same goal. But, to our knowledge, these finite Reynolds number corrections have not yet been corroborated by experimental or computational data. Here, numerical simulation data (del Álamo *et al.* 2004; Hoyas & Jiménez 2006) are employed for this purpose.

The asymptotic analysis is unusual because, due to the closure problem, the functions appearing in the asymptotic expansion will not be solved for. Instead, only the limiting behaviours of the inner and outer solutions are determined from the asymptotic matching, which can be accomplished without further modelling assumptions (Afzal 1976). Thus, the asymptotic behaviour of the mean velocity described here is just a consequence of the well-known multi-scale structure of the wall-layer. To demonstrate the ideas, a simplified version of the analysis is outlined below. As in the Millikan analysis, matching is done on an expansion for the velocity gradient, rather than on the velocity, and for simplicity, the asymptotic form suggested by the Millikan results is adopted:

$$\frac{\partial u^+}{\partial y^+} = \frac{1}{y^+} f_0\left(\frac{1}{y^+}\right) + \delta_1 f_1\left(\frac{1}{y^+}\right) + \dots \quad \text{inner}, \quad (4.1)$$

$$\frac{\partial u^+}{\partial y^+} = \frac{\epsilon}{\tilde{y}} F_0(\tilde{y}) + \frac{\Delta_1}{\tilde{y}} F_1(\tilde{y}) + \dots \quad \text{outer}. \quad (4.2)$$

The gauge functions δ_i and Δ_i are functions of the small parameter $\epsilon = 1/h^+$, and the outer variable is $\tilde{y} = \epsilon y^+$. For notational convenience, the inner functions f_i are expressed in terms of $1/y^+$, rather than y^+ . The matching conditions will apply in the limit of $y^+ \rightarrow \infty$ ($1/y^+ \rightarrow 0$), while $\tilde{y} \rightarrow 0$. Since the inner and outer solutions f_i and F_i will not be determined, they are represented in terms of a Taylor series about zero (essentially a Laurent series in y^+ for the inner solution). The values of f_i , F_i and their derivatives at zero will thus be undetermined constants (like the Karman constant κ). In pursuing this analysis, we implicitly assume that the functions are sufficiently regular at zero for the derivatives to exist. Matching is accomplished using the technique of van Dyke (1975) and is pursued here for three steps, with the following results at each step.

$$\text{Step 1: } F_0(0) = f_0(0) = \frac{1}{\kappa}. \quad (4.3)$$

$$\text{Step 2: } \delta_1 = \epsilon \quad f_1(0) = F'_0(0) = \alpha. \quad (4.4)$$

$$\text{Step 3: } \Delta_1 = \epsilon^2 \quad F_1(0) = f'_1(0) = \beta \quad f'_0 = 0. \quad (4.5)$$

The first matching step reproduces the results of Millikan and the constant is written $1/\kappa$ for consistency with the standard nomenclature. The resulting asymptotic forms for the inner and the outer expansions are obtained by replacing the f_i and F_i with the terms of their Taylor expansion that are determined by the matching. These can then be integrated in y to obtain the

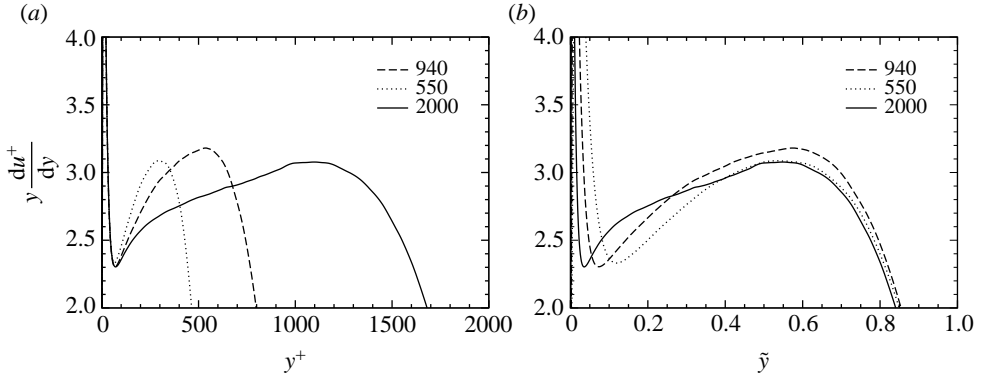


Figure 6. $y du^+ / dy$ from direct numerical simulation at $h^+ = 550, 940$ and 2000 .

refined overlap expressions:

$$u_i^+ = \left(\frac{1}{\kappa} + \frac{\beta}{h^+} \right) \ln y^+ + \frac{\alpha y^+}{h^+} + B_i, \tag{4.6}$$

$$u_o^+ - u_c^+ = \left(\frac{1}{\kappa} + \frac{\beta}{h^+} \right) \ln \tilde{y} + \alpha \tilde{y} + B_o. \tag{4.7}$$

In the context of this analysis, the integration constants B_i and B_o are, in general, Reynolds number-dependent, though κ , α and β are not. However, the data presented below indicates that this Reynolds number dependence should not be strong.

A nearly identical result was obtained by Afzal & Yajnik (1973), though they retained the possibility of a non-zero f_0 , by allowing F_1 to be singular at zero, which is not considered here because it violates our assumptions of the regularity of the functions at zero. However, such a singular term could arise if a y shift is introduced in the logarithmic law (Lindgren *et al.* 2004), which might extend the range of validity of the representation to somewhat smaller y . This possibility will not be explored here.

To evaluate the validity of the finite Reynolds number refinement of the logarithmic law described above, numerical simulations (del Álamo *et al.* 2004; Hoyas & Jiménez 2006) are used to determine the quantity $y(\partial u^+ / \partial y)$, which is plotted versus y^+ and \tilde{y} in figure 6. According to the above analysis, expressions for this quantity in inner and outer coordinates are

$$y \frac{\partial u^+}{\partial y} = \frac{1}{\kappa} + \frac{\alpha y^+}{h^+} + \frac{\beta}{h^+}, \tag{4.8}$$

$$y \frac{\partial u^+}{\partial y} = \frac{1}{\kappa} + \alpha \tilde{y} + \frac{\beta}{h^+}. \tag{4.9}$$

In the overlap region where these expressions apply, $y(\partial u^+ / \partial y)$, which would be a constant with value $1/\kappa$ in a log-layer, will be a line with slope of α/h^+ when plotted in inner units. In this way, a log-layer is approached at high h^+ as the slope of $y(\partial u^+ / \partial y)$ goes to zero in the overlap. In outer units, the slope of $y(\partial u^+ / \partial y)$ in the overlap region is independent of h^+ . In figure 6, it appears that the $h^+ = 940$ and $h^+ = 2000$ channels exhibit a straight region with these

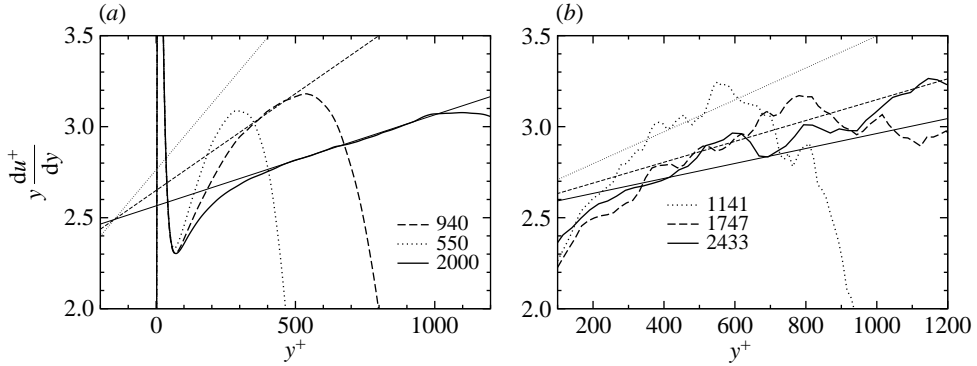


Figure 7. Zoomed-in view of $y(du^+/dy)$ from (a) direct numerical simulation for Reynolds numbers $h^+ = 550, 940$ and 2000 and (b) PIV measurements at Reynolds numbers $h^+ = 1141, 1747$ and 2433 . The thin lines are $y(du^+/dy)$ determined from equation (4.8), with constants $\alpha = 1.0$, $\beta = 150$ and $1/\kappa = 2.49$, which were determined from the simulation data in (a).

properties for $\tilde{y} < 0.45$ and $y^+ > 300$, which are thus the limits of applicability of the overlap expressions (4.8) and (4.9). The slope of the curves in the overlap region is $\alpha \approx 1.0$, which is estimated from the $h^+ = 2000$ case.

These limits are much larger than those commonly assumed and discussed in §2. However, recent experiments also suggest a much larger inner limit for the log layer, ranging from $y^+ \sim 200$ to 600 (Österlund *et al.* 2000; Zanoun *et al.* 2003; McKeon *et al.* 2004). Further in Wosnik *et al.* (2000), a Reynolds number-dependent mesolayer in the range $30 < h^+ < 300$ is postulated, with a log layer only evident beyond $y^+ \sim 300$, and Lindgren *et al.* (2004) propose that the apparent log layer breaks down for $y^+ < 200$ owing to a y offset in the logarithmic term.

The extension of the outer limit of the overlap representation to $\tilde{y} \approx 0.45$ is somewhat surprising, but it may be that including the next order term expands the range of applicability. For example, in the overlap range, the value of $y(du^+/dy)$, which can be considered the local value of $1/\kappa$, varies by approximately 20% (independent of h^+). If one insisted on a region with negligible variation of κ (i.e. a true logarithmic layer), one would likely choose a more limited range of \tilde{y} .

The values of κ and β in the channel are estimated from the numerical simulation profiles at $h^+ = 940$ and 2000 (figure 7a). The lines described by (4.8) intersect at the point $y^+ = -\beta/\alpha \approx -150$, $y(du^+/dy) = 1/\kappa \approx 2.49$. The parameters are thus estimated to be $\kappa \approx 0.40$ and $\beta \approx 150$. These estimates must be considered preliminary, since the overlap region is marginal at $h^+ = 940$. There are also statistical uncertainties in $y(du^+/dy)$ at large \tilde{y} , estimated to be as high as 0.04 in the $h^+ = 2000$ case, leading to uncertainties of order ± 0.02 , ± 0.1 and ± 40 in κ , α and β , respectively. The agreement with the standard value of κ may thus be coincidental. In addition, (4.8) is shown in figure 7a evaluated for $h^+ = 550$, and it does not approach the $h^+ = 550$ curve. This Reynolds number is too low for the flow to exhibit an overlap region, since, in this case, $y^+ = 300$ is at $\tilde{y} = 0.54 > 0.45$.

Experimental profiles that can be meaningfully differentiated are difficult to obtain, which is probably why the $y(du^+/dy)$ diagnostic has not often been used (exceptions include Zanoun *et al.* (2003); Lindgren *et al.* (2004)). However, the mean velocity data from the experiments of Natrajan & Christensen (2006) are

just smooth enough to yield meaningful derivatives, and $y(du^+/dy)$ from this data is shown in figure 7*b*. Assuming that the magnitude of the fluctuations in these curves is representative of the uncertainty in $y(du^+/dy)$, it appears that the experimental profiles are consistent (within the uncertainties) with (4.8) and the values of the coefficients determined above. The data of Zanon *et al.* (2003) produce much noisier values of $y(du^+/dy)$ (not shown), but they are also consistent (i.e. within the noise band) with (4.8) and the constants given above.

The analysis and simulation results presented above suggest that the log-layer refinement (4.8–4.9) is an accurate representation of finite Reynolds number effects in the channel. However, to convincingly demonstrate this and refine the associated constants and limits of applicability, reliable data at Reynolds numbers $h^+ \approx 4000$ or higher are needed. At this Reynolds number, the asymptotic scaling described here should be unambiguous, so that much higher Reynolds numbers should not be required to develop dynamic models of the logarithmic layer of the type described in §3. Direct numerical simulations at these Reynolds numbers should be possible in the next few years.

While the current analysis was performed for channel flow, the approach is generally applicable to wall-bounded shear flows (e.g. pipes and boundary layers), though it would be somewhat more complicated in a boundary layer (Mellor 1972). In the context of the current analysis, there is no reason to expect universality of the constants, and indeed the superpipe data of Zagarola *et al.* (1997) suggest a value of $\alpha \approx 2.5$, while it appears that $\alpha \approx 0$ in the boundary layer of Österlund *et al.* (2000) (a careful analysis of the available data would be useful to confirm this). The universality of κ between the boundary layer and channel is also of interest, but for now, statistical uncertainties make the value of $\kappa = 0.4$ determined here indistinguishable from the value of 0.384 in the boundary layer of Österlund *et al.* (2000). In any case, a possible small discrepancy in κ may be less significant than the apparent lack of universality in α .

(*b*) Kinematics and dynamics of log-layer turbulence

The simulations of del Álamo *et al.* (2004) and Hoyas & Jiménez (2006), as well as corresponding advances in experimental methods, have already greatly improved our kinematic understanding of the structures in the logarithmic layer. For example, it is known that there is a self-similar hierarchy of compact ejections extending from the buffer layer into the outer flow, within which the vorticity is more intense than elsewhere. They are associated with extremely long, conical, low-velocity regions in the logarithmic layer (del Álamo *et al.* 2006), ‘wakes’, which agree well with the energy-containing structures of the streamwise velocity spectrum. The arrangement is reminiscent of the association of vortices and streaks in the buffer layer, but at a much larger scale. It is also known that the low-velocity regions are almost identical to the transient-growth structures forced on the mean velocity profile by a concentrated ejection (del Álamo & Jiménez 2006), but that whatever is causing them does not grow directly from the buffer layer. The spectra of flows in which the buffer region has been purposefully destroyed are essentially identical to those over smooth walls (Flores & Jiménez 2006).

We know less about how the ejections are created, although there are indications that their association with the low-velocity regions goes both ways. The wakes are seen when the statistics are conditioned on the ejections, but the

lifetimes of the observed ejections are too short for them to be the origin of the wakes (del Álamo & Jiménez 2003). The knowledge that we are gaining from the present simulations is, however, essentially kinematic. Numerical experiments to probe the dynamics of log-layer turbulence will likely be required to go beyond that level of understanding.

5. Conclusions

We have briefly reviewed the present state of understanding of the dynamics of turbulent flows near smooth walls. This is a subject that, like most others in turbulence, is not fully closed, but which has evolved in the last two decades from empirical observations to relatively coherent theoretical models. It is also one of the first cases in turbulence, perhaps together with the structure of small-scale vorticity in isotropic turbulence, in which the key technique has been the numerical simulation of the flow. The reason is that the Reynolds numbers of the important structures are low, and therefore accessible to computation, while experiments are difficult. For example, the spanwise spacing of the streaks is of the order of $z^+ = 100$, which is less than a millimetre in most experiments, but we have seen that it is well predicted by the range of parameters in which the associated equilibrium solutions exist. We have seen that the larger structures coming from the outside flow interfere only weakly with the near-wall region, because the local dynamics are intense enough to be always dominant. The streak spacing just mentioned has been observed up to the highest Reynolds numbers of the atmospheric boundary layer (Klewicky *et al.* 1995).

On the other hand, the thinness of the layer in which this dynamics takes place makes the flow very sensitive to small perturbations at the wall. Roughness elements with heights of the order of a few wall units, micrometres in a large pipe, completely destroy the delicate cycle that we have described and can increase the friction coefficient by a factor of two or more (Jiménez 2004). Conversely, it only takes a polymer concentration of a few parts per million in the near-wall region to decrease the drag coefficient by 40% (McComb 1990). The same is true of the control strategies based on the manipulation of the near-wall structures (Choi *et al.* 1994; Jiménez 1994).

In the logarithmic layer, recent numerical simulations have been extremely valuable in determining scaling and kinematic characteristics. For example, validating and parameterizing a finite Reynolds number correction to the logarithmic profile has allowed the occurrence and extent of the overlap region in a channel at finite Reynolds numbers to be determined. As important as these refinements are to describing the logarithmic layer and interpreting experiments and simulations, they tell us little about the workings of the turbulence. After all, the asymptotic analysis that leads to the logarithmic law and to the finite Reynolds number correction relies only on the existence of an inner and outer length-scale, not on the dynamic properties of the turbulence.

In essence, numerical simulations have so far allowed us to observe the structure of the logarithmic layer, but not its dynamics. The problem is one of cost, and was shared by the original low-Reynolds number simulations that eventually led to the understanding of the buffer layer. The simulation in Hoyas & Jiménez (2006) took six months on 2100 supercomputer processors. It took a similar time to run the

simulation in Kim *et al.* (1987) at $h^+ = 180$. As long as each numerical experiment takes such long times, it is only possible to observe the results, and simulations are little more than better-instrumented laboratory experiments.

As computers improve, other things become possible. When the low-Reynolds number simulations of the 1980s became roughly 100 times cheaper in the 1990s, it became possible to experiment with them in ways that were impossible in the laboratory. The ‘conceptual’ simulations that led to the results in §3 were of this kind. The perturbed-wall simulations cited above by Flores & Jiménez (2006) are one of the first examples of this type of simulations for the logarithmic layer, but their Reynolds numbers are still only marginal, and they are in any case conceptually similar to flows over rough walls.

There is, however, no reason to believe that computer improvements have stopped, and the next decade will bring the cost of the simulations of the logarithmic layer to the level at which dynamical experiments should become commonplace. It is only then that we can expect a dynamical theory for this part of the flow to emerge from simulations. The motivation for such research is both theoretical and technological. The cascade of momentum across the range of scales in the logarithmic layer is probably the first three-dimensional self-similar cascade that will be accessible to computational experiments. Its simplifying feature is the alignment of most of the net transfer along the direction normal to the wall. The main practical drive is probably large-eddy simulation, in which the momentum transfer across scales in the inertial range has to be modelled for the method to be practical (Jiménez & Moser 2000). Only by understanding the structures involved, we will be sure of how to accomplish that.

The preparation of this paper was supported in part by the CICYT grant DPI2003-03434 (J.J.) and NSF grant CTS-0352552 (R.D.M.). We are deeply indebted to J.C. del Álamo, O. Flores, S. Hoyas, G. Kawahara, M.P. Simens and K. T. Christensen for providing most of the data used in the figures.

References

- Afzal, N. 1976 Millikan’s argument at moderately large Reynolds number. *Phys. Fluids* **19**, 600–602. (doi:10.1063/1.861498)
- Afzal, N. & Yajnik, K. 1973 Analysis of turbulent pipe and channel flows at moderately large Reynolds number. *J. Fluid Mech.* **61**, 23–31. (doi:10.1017/S0022112073000546)
- Aubry, N., Holmes, P., Lumley, J. L. & Stone, E. 1988 The dynamics of coherent structures in the wall region of a turbulent boundary layer. *J. Fluid Mech.* **192**, 115–173. (doi:10.1017/S0022112088001818)
- Bakewell, H. P. & Lumley, J. L. 1967 Viscous sublayer and adjacent wall region in turbulent pipe flow. *Phys. Fluids* **10**, 1880–1889. (doi:10.1063/1.1762382)
- Bradshaw, P. 1967 Inactive motions and pressure fluctuations in turbulent boundary layers. *J. Fluid Mech.* **30**, 241–258. (doi:10.1017/S0022112067001417)
- Bradshaw, P. & Koh, Y. 1981 A note on Poisson’s equation for pressure in a turbulent flow. *Phys. Fluids* **24**, 777. (doi:10.1063/1.863442)
- Brown, G. & Roshko, A. 1974 On the density effects and large structure in turbulent mixing layers. *J. Fluid Mech.* **64**, 775–816. (doi:10.1017/S002211207400190X)
- Choi, H., Moin, P. & Kim, J. 1994 Active turbulence control and drag reduction in wall-bounded flows. *J. Fluid Mech.* **262**, 75–110. (doi:10.1017/S0022112094000431)
- Darcy, H. 1854 Recherches expérimentales relatives au mouvement de l’eau dans les tuyaux. *Mém. Savants Etrang. Acad. Sci. Paris* **17**, 1–268.

- DeGraaf, D. B. & Eaton, J. K. 2000 Reynolds number scaling of the flat-plate turbulent boundary layer. *J. Fluid Mech.* **422**, 319–346. (doi:10.1017/S0022112000001713)
- del Álamo, J. C. & Jiménez, J. 2003 Spectra of very large anisotropic scales in turbulent channels. *Phys. Fluids* **15**, L41–L44. (doi:10.1063/1.1570830)
- del Álamo, J. C. & Jiménez, J. 2006 Linear energy amplification in turbulent channels. *J. Fluid Mech.* **559**, 205–213. (doi:10.1017/S0022112006000607)
- del Álamo, J. C., Jiménez, J., Zandonade, P. & Moser, R. D. 2004 Scaling of the energy spectra of turbulent channels. *J. Fluid Mech.* **500**, 135–144. (doi:10.1017/S002211200300733X)
- del Álamo, J. C., Jiménez, J., Zandonade, P. & Moser, R. D. 2006 Self-similar vortex clusters in the logarithmic region. *J. Fluid Mech.* **561**, 329–358. (doi:10.1017/S0022112006000814)
- Flores, O. & Jiménez, J. 2006 Effect of wall-boundary disturbances on turbulent channel flows. *J. Fluid Mech.* **566**, 357–376. (doi:10.1017/S0022112006001534)
- Hagen, G. H. L. 1839 Über den Bewegung des Wassers in engen cylindrischen Röhren. *Poggendorfs Ann. Physik Chemie* **46**, 423–442.
- Hamilton, J. M., Kim, J. & Waleffe, F. 1995 Regeneration mechanisms of near-wall turbulence structures. *J. Fluid Mech.* **287**, 317–248. (doi:10.1017/S0022112095000978)
- Hoyas, S. & Jiménez, J. 2006 Scaling of the velocity fluctuations in turbulent channels up to $Re_\tau=2003$. *Phys. Fluids* **18**, 011 702. (doi:10.1063/1.2162185)
- Hu, Z., Morley, C. & Sandham, N. 2006 Wall pressure and shear stress spectra from direct simulations of channel flow. *AIAA J.* **44**, 1541–1549. (doi:10.2514/1.17638)
- Jeong, J., Hussain, F., Schoppa, W. & Kim, J. 1997 Coherent structures near the wall in a turbulent channel flow. *J. Fluid Mech.* **332**, 185–214.
- Jiménez, J. & Moin, P. 1991 The minimal flow unit in near-wall turbulence. *J. Fluid Mech.* **225**, 221–240. (doi:10.1017/S0022112091002033)
- Jiménez, J. & Moser, R. D. 2000 LES: where are we and what can we expect? *AIAA J.* **38**, 605–612.
- Jiménez, J. & Pinelli, A. 1999 The autonomous cycle of near wall turbulence. *J. Fluid Mech.* **389**, 335–359. (doi:10.1017/S0022112099005066)
- Jiménez, J. & Simens, M. P. 2001 Low-dimensional dynamics in a turbulent wall flow. *J. Fluid Mech.* **435**, 81–91. (doi:10.1017/S0022112001004050)
- Jiménez, J. 1994 On the structure and control of near wall turbulence. *Phys. Fluids* **6**, 944–953. (doi:10.1063/1.868327)
- Jiménez, J. 2004 Turbulent flows over rough walls. *Annu. Rev. Fluid Mech.* **36**, 173–196. (doi:10.1146/annurev.fluid.36.050802.122103)
- Jiménez, J., del Álamo, J. C. & Flores, O. 2004 The large-scale dynamics of near-wall turbulence. *J. Fluid Mech.* **505**, 179–199. (doi:10.1017/S0022112004008389)
- Jiménez, J., Kawahara, G., Simens, M. P., Nagata, M. & Shiba, M. 2005 Characterization of near-wall turbulence in terms of equilibrium and ‘bursting’ solutions. *Phys. Fluids* **17**, 015 105. (doi:10.1063/1.1825451)
- Kawahara, G. & Kida, S. 2001 Periodic motion embedded in plane Couette turbulence: regeneration cycle and burst. *J. Fluid Mech.* **449**, 291–300. (doi:10.1017/S0022112001006243)
- Kawahara, G., Jiménez, J., Uhlmann, M. & Pinelli, A. 2003 Linear instability of a corrugated vortex sheet—a model for streak instability. *J. Fluid Mech.* **483**, 315–342. (doi:10.1017/S002211200300421X)
- Kim, H. T., Kline, S. J. & Reynolds, W. C. 1971 The production of turbulence near a smooth wall in a turbulent boundary layer. *J. Fluid Mech.* **50**, 133–160. (doi:10.1017/S0022112071002490)
- Kim, J., Moin, P. & Moser, R. D. 1987 Turbulence statistics in fully developed channel flow at low Reynolds number. *J. Fluid Mech.* **177**, 133–166. (doi:10.1017/S0022112087000892)
- Klewicki, J. C., Metzger, M. M., Kelner, E. & Thurlow, E. 1995 Viscous sublayer flow visualizations at $R_\delta \approx 1,500,000$. *Phys. Fluids* **7**, 857–863. (doi:10.1063/1.868763)
- Kolmogorov, A. N. 1941 The local structure of turbulence in incompressible viscous fluids a very large Reynolds numbers. *Dokl. Akad. Nauk. SSSR* **30**, 301–305. Reprinted in *Proc. R. Soc. A* **434**, 9–13 (1991). (doi:10.1098/rspa.1991.0075)

- Lindgren, B., Österlund, J. M. & Johansson, A. V. 2004 Evaluation of scaling laws derived from Lie group symmetry methods in zero-pressure gradient turbulent boundary layers. *J. Fluid Mech.* **502**, 127–152. (doi:10.1017/S0022112003007675)
- McComb, W. 1990 *The physics of fluid turbulence*. Oxford, UK: Oxford University Press.
- McKeon, B. J., Li, J., Jiang, W., Morrison, J. F. & Smits, A. J. 2004 Further observations on the mean velocity distribution in fully developed pipe flow. *J. Fluid Mech.* **501**, 135–147. (doi:10.1017/S0022112003007304)
- Mellor, G. L. 1972 The large Reynolds number asymptotic theory of turbulent boundary layers. *Int. J. Eng. Sci.* **10**, 851–873. (doi:10.1016/0020-7225(72)90055-9)
- Millikan, C. M. 1938 A critical discussion of turbulent flows in channels and circular tubes. In *Proc. 5th Int. Congress of Applied Mechanics*, pp. 386–392. New York, NY: Wiley.
- Morrison, W. R. B., Bullock, K. J. & Kronauer, R. E. 1971 Experimental evidence of waves in the sublayer. *J. Fluid Mech.* **47**, 639–656. (doi:10.1017/S0022112071001290)
- Nagata, M. 1990 Three-dimensional finite-amplitude solutions in plane Couette flow: bifurcation from infinity. *J. Fluid Mech.* **217**, 519–527. (doi:10.1017/S0022112090000829)
- Natrajan, V. K. & Christensen, K. T. 2006 The role of coherent structures in subgrid-scale energy transfer within the log layer of wall turbulence. *Phys. Fluids* **18**, 065–104. (doi:10.1063/1.2206811)
- Österlund, J. M., Johansson, A. V., Nagib, H. M. & Hites, M. 2000 A note on the overlap region in turbulent boundary layers. *Phys. Fluids* **12**, 1–4. (doi:10.1063/1.870250)
- Phillips, W. R. C. 1987 The wall region of a turbulent boundary layer. *Phys. Fluids* **30**, 2354–2360. (doi:10.1063/1.866125)
- Reddy, S. C., Schmid, P. J., Baggett, J. S. & Henningson, D. S. 1998 On stability of streamwise streaks and transition thresholds in plane channel flows. *J. Fluid Mech.* **365**, 269–303. (doi:10.1017/S0022112098001323)
- Robinson, S. K. 1991 Coherent motions in the turbulent boundary layer. *Annu. Rev. Fluid Mech.* **23**, 601–639. (doi:10.1146/annurev.fl.23.010191.003125)
- Schoppa, W. & Hussain, F. 2002 Coherent structure generation in near-wall turbulence. *J. Fluid Mech.* **453**, 57–108. (doi:10.1017/S002211200100667X)
- Sirovich, L. & Zhou, X. 1994 Dynamical model of wall-bounded turbulence. *Phys. Rev. Lett.* **72**, 340–343. (doi:10.1103/PhysRevLett.72.340)
- Smith, C. R. & Metzler, S. P. 1983 The characteristics of low speed streaks in the near wall region of a turbulent boundary layer. *J. Fluid Mech.* **129**, 27–54. (doi:10.1017/S0022112083000634)
- Swearingen, J. D. & Blackwelder, R. F. 1987 The growth and breakdown of streamwise vortices in the presence of a wall. *J. Fluid Mech.* **182**, 255–290. (doi:10.1017/S0022112087002337)
- Tennekes, H. & Lumley, J. L. 1972 *A first course in turbulence*. Cambridge, MA: MIT Press.
- Toh, S. & Itano, T. 2001 On the regeneration mechanism of turbulence in the channel flow. In *Proc. Iutam Symp. on Geometry and Statistics of Turbulence* (eds T. Kambe & T. Muiyauchi), pp. 305–310. Dordrecht, the Netherlands: Kluwer.
- Toh, S. & Itano, T. 2003 A periodic-like solution in channel flow. *J. Fluid Mech.* **481**, 67–76. (doi:10.1017/S0022112003003768)
- Townsend, A. 1976 *The structure of turbulent shear flow*, 2nd edn. Cambridge, UK: Cambridge University Press.
- van Dyke, M. 1975 *Perturbation methods in fluid mechanics*. Stanford, CA: Parabolic Press.
- Waleffe, F. 1997 On a self-sustaining process in shear flows. *Phys. Fluids* **9**, 883–900. (doi:10.1063/1.869185)
- Waleffe, F. 1998 Three-dimensional coherent states in plane shear flows. *Phys. Rev. Lett.* **81**, 4140–4143. (doi:10.1103/PhysRevLett.81.4140)
- Waleffe, F. 2001 Exact coherent structures in channel flow. *J. Fluid Mech.* **435**, 93–102. (doi:10.1017/S0022112001004189)
- Waleffe, F. 2003 Homotopy of exact coherent structures in plane shear flows. *Phys. Fluids* **15**, 1517–1534. (doi:10.1063/1.1566753)

- Wosnik, M., Castillo, L. & George, W. K. 2000 A theory for turbulent pipe and channel flows. *J. Fluid Mech.* **421**, 115–145. (doi:10.1017/S0022112000001385)
- Yajnik, K. S. 1970 Asymptotic theory of turbulent shear flows. *J. Fluid Mech.* **42**, 411–427. (doi:10.1017/S0022112070001350)
- Zagarola, M. V., Perry, A. E. & Smits, A. J. 1997 Log laws or power laws: the scaling in the overlap region. *Phys. Fluids* **9**, 2094–2100. (doi:10.1063/1.869328)
- Zanoun, E.-S., Durst, F. & Nagib, H. 2003 Evaluating the law of the wall in two-dimensional fully developed turbulent channel flows. *Phys. Fluids* **15**, 3079–3089. (doi:10.1063/1.1608010)